Research Article

Nano Research
2023, 16(4): 5042–5046

ISSN 1998-0124 CN 11-5974/O4
https://doi.org/10.1007/s12274-022-5241-2

Laser trimming for lithography-free fabrications of MoS_2 devices

Yong Xie[1,2] (✉), Onur Çakıroğlu[2], Wenshuai Hu[1], Kexin He[1], Sergio Puebla[2], Thomas Pucher[2], Qinghua Zhao[2], Xiaohua Ma[1], Carmen Munuera[2], and Andres Castellanos-Gomez[2] (✉)

[1] *Key Laboratory of Wide Band-Gap Semiconductor Technology, School of Advanced Materials and Nanotechnology, Xidian University, Xi'an 710071, China*

[2] *Materials Science Factory, Instituto de Ciencia de Materiales de Madrid, Consejo Superior de Investigaciones Científicas, 28049 Madrid, Spain*

Received: 18 July 2022 / **Revised:** 13 October 2022 / **Accepted:** 25 October 2022

ABSTRACT

Single-layer MoS_2 produced by mechanical exfoliation is usually connected to thicker and multilayer regions. We show a facile laser trimming method to insulate single-layer MoS_2 regions from thicker ones. We demonstrate, through electrical characterization, that the laser trimming method can be used to pattern single-layer MoS_2 channels with regular geometry and electrically disconnected from the thicker areas. Scanning photocurrent microscope further confirms that in the as-deposited flake (connected to a multilayer area) most of the photocurrent is being generated in the thicker flake region. After laser trimming, scanning photocurrent microscopy shows how only the single-layer MoS_2 region contributes to the photocurrent generation. The presented method is a direct-write and lithography-free (no need of resist or wet chemicals) alternative to reactive ion etching process to pattern the flakes that can be easily adopted by many research groups fabricating devices with MoS_2 and similar two-dimensional materials.

KEYWORDS

2D materials, transition metal dichalcogenides, laser trimming, differential reflectance

1 Introduction

Two-dimensional (2D) layered transition metal dichalcogenide (TMDC) semiconductors (e.g., MoS_2) have attracted significant attention for their potential in future electronics and optoelectronics applications due to their superior electrical, optical, mechanical, and magnetic properties [1–3]. Mechanically exfoliated flakes yield the best quality material so far but single-layer regions are typically connected to thicker areas. However, single-layer TMDC is typically the most interesting part in term of direct band gap and unique physical properties [4]. In order to ensure that electrical transport occurs through the single-layer region, a complex design of electrodes can be done sometimes or reactive ion etching process can be carried out to pattern the single-layer flake and remove the thicker region. However, atomically thin TMDCs are found to be very sensitive to the traditional lithographic process, such as photolithography and E-beam lithography [5]. The contamination and residues from photoresist can dramatically influence the electrical properties of the devices. The threshold voltage of a MoS_2 field-effect transistor shifted about 80 V towards positive after the E-beam lithography process [6]. Therefore, development of fabrication protocols that enable device fabrication minimizing (or even eliminating) the need of resist-based lithography techniques is important for the advancement of the field.

In this work, a laser trimming process based on the commercial Raman system was utilized to isolate the monolayer part of MoS_2 from the multilayered part. Due to the MoS_2 thermal conductivity anisotropy ($k_{\parallel}$ = 85–110 $W \cdot m^{-1} \cdot K^{-1}$ and $k^{\perp}$ = 2 $W \cdot m^{-1} \cdot K^{-1}$) [7–10], the heat irradiated from the external laser can be hardly dissipated out-of-plane, which could cause localized high temperature. This has been used to thin down the bulk MoS_2 to the monolayer limit on-demand with a spatial resolution of 200 nm [11] and we now use the same effect to pattern MoS_2 flakes without the need of using reactive ion etching. The electrical measurements show a decrease of the drain-source current while keeping rather constant electrical conductivity, consistent with the reduction of the effective semiconductor channel area. The spatially resolved photocurrent measurements showed that for the as-deposited flake, most of the photocurrent was generated in the few-layer thick part, while the laser trimmed flake demonstrates how all the photocurrent was generated at the single-layer part of the device. Furthermore, wavelength dependent photocurrent measurements show that in the laser-trimmed device the photocurrent presents a peak corresponding to the A exciton of single-layer MoS_2, indicating that the single-layer region has been effectively disconnected from the multilayer MoS_2, which do not contribute anymore to the transport.

2 Experimental details

2.1 Deterministic dry transferring of MoS_2 onto electrodes on SiO_2/Si

The bulk MoS_2 crystal was first exfoliated with a Scotch tape (Magic Tape by 3M). The flake from the Scotch tape was then further thinned down with blue Nitto tape (Nitto Denko Co., SPV 224P). A polydimethylsiloxane (PDMS) stamp (Gel-Fim® WF ×4

Address correspondence to Yong Xie, yxie@xidian.edu.cn; Andres Castellanos-Gomez, andres.castellanos@csic.es

6.0mil by Gelpak) was placed on top of the Nitto tape and gently pressed by a cotton swab. After that the PDMS was quickly detached from the Nitto tape and examined under an optical microscope. Flakes as thin as monolayer (1L) can be distinguished by transmittance or reflectance mode of the optical microscope [12].

After finding a 1L MoS_2 with suitable shape and size, longer than 40 μm, we employ an all dry transfer method to transfer the flake onto SiO_2/Si substrate with Ti/Au electrodes [13]. The PDMS was cut and placed on a glass slide. After that the glass slide was mounted on a three-dimensional micromanipulator. Then the flake on PDMS was deterministically transferred on the Ti/Au electrodes.

This method to contact the MoS_2 flakes results advantageous as it has been shown that evaporation of Au can damage the surface of MoS_2 up to four layers, inducing defects that lead to Fermi level pinning [14]. Thereby, different methods are developed to avoid the evaporation process in two-dimensional devices. Atomically flat metal thin films can be transferred onto two-dimensional semiconductors, creating an interface that could reach the Schottky–Mott limit [15]. An all dry transfer process like the one used in this work to fabricate MoS_2 devices has been widely adopted by others to prevent the contamination and damage from the standard semiconductor process [2, 13]. However, as inheritably from the exfoliation method, the single-layer part of the flake is typically attached with a bulk part, which could be a highly conductive channel diverting part of the current flow from the single-layer part.

2.2 Laser trimming of MoS_2 devices

After the dry transfer, the MoS_2 device was laser trimmed by a commercial Raman system (MonoVista CRS +) with a laser spot size below 1 μm using a 532 nm laser. First, the MoS_2 device was carefully aligned with the scanning direction of the laser with the 100× (NA 0.90) objective lens. The scanning direction is either parallel or perpendicular to the Ti/Au electrodes. Second, an optimized laser power and exposure time were chosen to trim the area by using either the line scan mode or the XY mapping mode. Typical step used in the laser trimming is 0.2 μm. Typical laser power is from 10 to 20 mW, and the typical laser exposure time is 10 s. To laser trim very thick MoS_2 flakes, multiple laser trimming steps could be performed.

2.3 Electrical and optoelectronics measurements

Prior to electrical characterization, the devices were annealed in vacuum 5 × 10^{-6} mbar at about 200 °C for 2 h. Transfer and output characteristics of back gated MoS_2 transistors were recorded using a home-built probe station system. A Keithley 2450 source meter unit was used to apply the source-drain voltage and measure the source-drain current. Two programmable TENMA (72-2715) benchtop power supply units were used to apply the positive and negative gate voltage sharing the same ground with the source electrode. The wavelength dependence of the photocurrent of the device was performed with the same electrical setup with illumination from the BENTHAM broadband tunable light source (TLS120Xe) connected with a multimode optical fiber to a zoom-lens system to project a circular spot of 400 μm radius onto the device. The photocurrent mapping was measured using a home built scanning setup with Optogear 650 nm laser as shown in literature before [15].

3 Results and discussion

Differential reflectance spectroscopy was used to probe the number of layers of MoS_2 flakes on PDMS before the dry transfer [16]. As shown in Fig. 1(f), the blue dotted marked region of the 1L MoS_2 flake has the A exciton and B exciton peaks at 1.91 and 2.06 eV, respectively. The bilayer (2L) MoS_2 region, on the other hand, has its A exciton, interlayer (IL) exciton, and B exciton peaks at 1.88, 1.95, and 2.05 eV.

A laser trimming process was used to cut through the multilayer region of the MoS_2 flake, as shown in Fig. 2. Laser was scanned with a laser power (P_{Laser}) ranging from 10 to 20 mW (regions 1L and 2L in Fig. 2(d) and Fig. S3 in the Electronic Supplementary Material (ESM)), following the dashed lines to isolate the single-layer MoS_2 part from the multilayer part and to disconnect the multilayer part from the source-drain electrodes. With the hBN capping, a higher laser power is needed to laser trimming the underneath and nearby MoS_2 flake, as shown in Fig. S3 and Table S2 in the ESM. The laser cut lines can be easily resolved under the optical microscope.

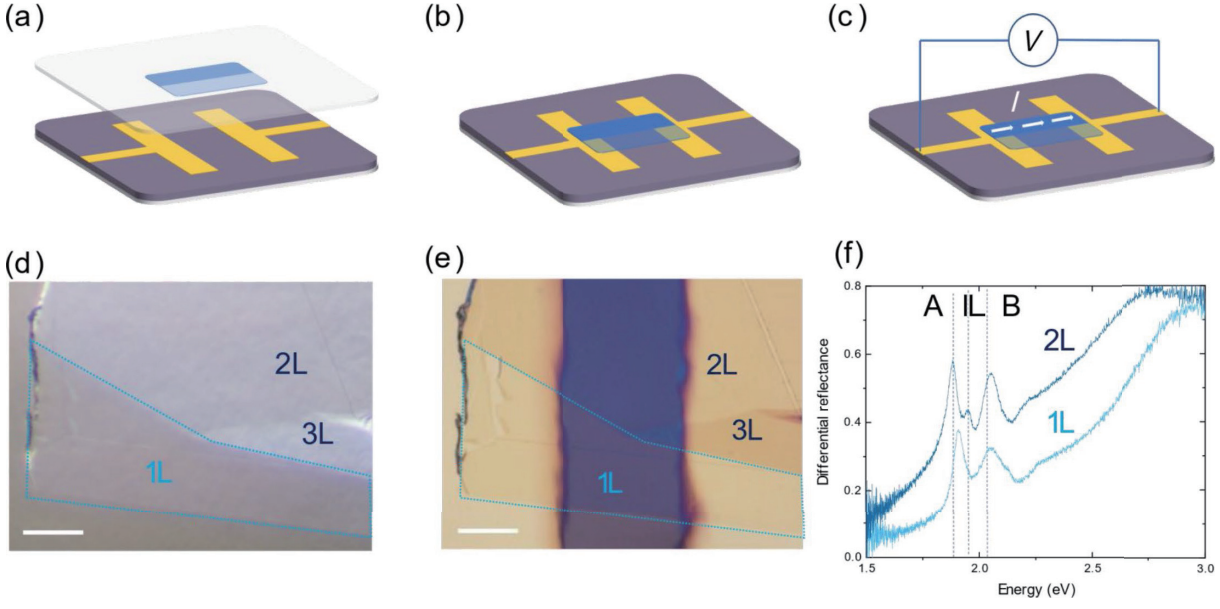

Figure 1 Dry transfer process of 1L/multilayer MoS_2 onto Au electrodes. (a) Dry transferring a MoS_2 flake onto Au using a PDMS stamp. (b) The MoS_2 flake on Au electrodes after removing the PDMS. (c) The current mainly passing through the thicker part of the MoS_2 flakes by applying source drain voltage. (d) Optical micrograph 1L/multilayer MoS_2 on PDMS. (e) Optical micrograph of the as-fabricated MoS_2 device. (f) Differential reflectance spectra of the 1L/2L part of MoS_2 in (d). The A, B, and IL exciton peaks are highlighted. Scale bars: 10 μm.

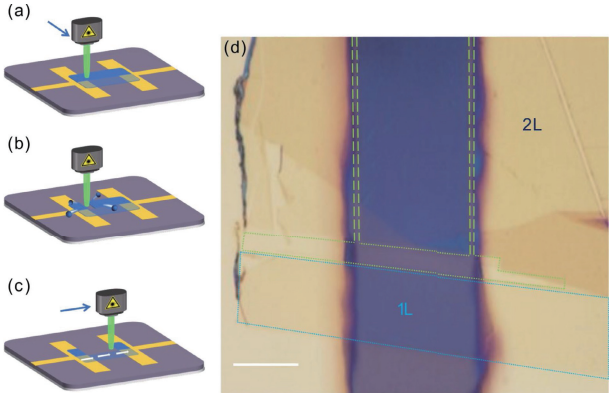

Figure 2 Laser trimming process of 1L/multilayer MoS_2 device (device B) using 532 nm green laser. (a) and (b) Laser scanning to separate the 1L from the multilayer part of MoS_2 device (device B) and to disconnect the multilayer part from the electrodes. (c) The current can only pass through the 1L part after laser trimming. (d) The corresponding 1L MoS_2 device (same as in Fig. 1(e)) after laser trimming. The blue dotted rectangular marks the 1L MoS_2 separated from the multilayer part. The green dotted lines mark the laser trimming area. Scale bar: 10 μm.

For comparison, a single layer MoS_2 device (device A) is fabricated by the all dry transfer method. Photoresist was spin-coated on the surface of the device, followed by cleaning with acetone and isopropanol. The electrical measurements of the device before and after photoresist coating were shown in Fig. S6 in the ESM. We can see the threshold voltage of device A shifts to a more negative voltage, indicating a strong doping effect. Therefore, it is very beneficial to adopt our photoresist and chemical free process for the 2D materials. To explore the electrical properties of the MoS_2 device before and after laser trimming, transfer and output measurements were compared for the back-gated MoS_2 transistor, as shown in Fig. 3. The current–voltage (I–V) characteristics show linear relationship in the −1 to 1 V range, which show the reduced Schottky barrier after the annealing for our devices fabricated by all dry transfer method [17]. The transfer characteristics in Fig. 3 show the n-type conduction of the MoS_2 back-gated transistor. The ON–OFF ratio of the ON current and the OFF current before laser trimming can reach five orders of magnitude. After laser trimming, the current dropped to about one fifth of the original current with the same bias voltage for device B (Fig. S4(d) in the ESM). This can be explained by the reduction of the channel width. Indeed the current density in the channel (current divided by channel width) did not change much after the laser thinning (Figs. S5 and S6 in the ESM). The transfer characteristic demonstrates the similar trend with the output curves. The threshold voltage with the forward gate sweep voltage slightly shifted from −17 to −16 V for device B (Figs. S5 and S6 in the ESM), and from −25 to −16 V for device C (Fig. 3(d)). The mobility (μ_{FE}) can be extracted from the transfer curve of the back-gated transistor with Eq. (1) [18]

$$\mu_{FE} = \frac{dI_{DS}}{dV_{GS}} \frac{L}{W} \frac{1}{C_g \cdot V_{DS}} \quad (1)$$

where I_{DS}, V_{DS}, and V_{GS} are the source-drain current, source-drain voltage, and the gate-source voltage, C_g is the capacitance of the oxide, and L and W are the length and width of the transistor. The calculated field effect mobility slightly increased from 0.36 to 0.79 $cm^2 \cdot V^{-1} \cdot s^{-1}$ for device B and 24.80 to 27.87 $cm^2 \cdot V^{-1} \cdot s^{-1}$ for device C, which could be attributed to further thermal annealing during the high power laser treatment that might lead to improved metal–semiconductor contacts [14].

In order to further probe the effectiveness of the laser trimming methods, we characterized one device with spatially resolved scanning photocurrent and photocurrent spectroscopy before and after laser trimming, as shown in Fig. 4. Before laser trimming, the multilayered part of the flake contributes largely to the photocurrent generation (Fig. 4(b)), as expected from the larger optical absorption of the multilayer flake with respect to the single-layer. Moreover, the wavelength dependent photocurrent spectrum has two prominent peaks located at 660 and 605 nm, in excellent agreement with the A and B exciton peaks of bilayer MoS_2 in Fig. 1(f), and the photocurrent does not drop abruptly to zero for photons with energy higher than the A exciton. These two observations thus indicate that most of the photocurrent is being generated at the bilayer region of the flake. After laser trimming,

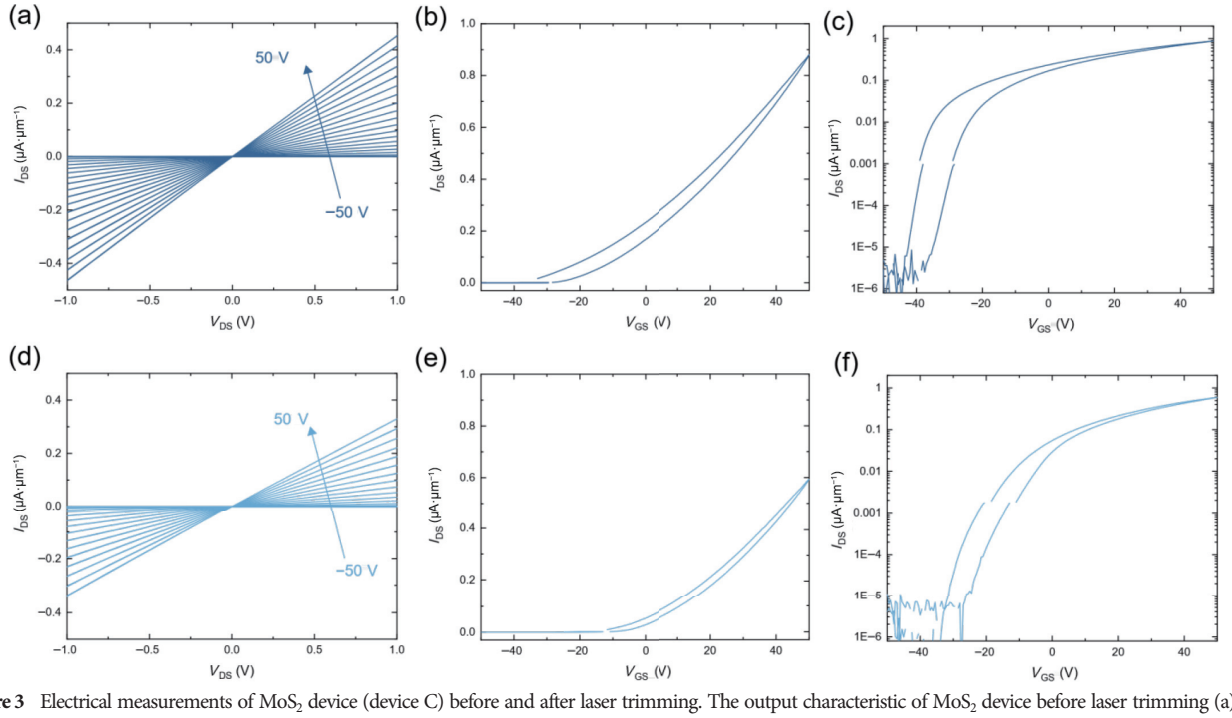

Figure 3 Electrical measurements of MoS_2 device (device C) before and after laser trimming. The output characteristic of MoS_2 device before laser trimming (a) and after laser trimming (d). The gate voltages are swept from −50 to 50 V with a step of 5 V. The transfer characteristics of MoS_2 device before laser trimming ((b) and (c)) and after laser trimming ((e) and (f)). The source drain bias voltage applied here is 1 V.

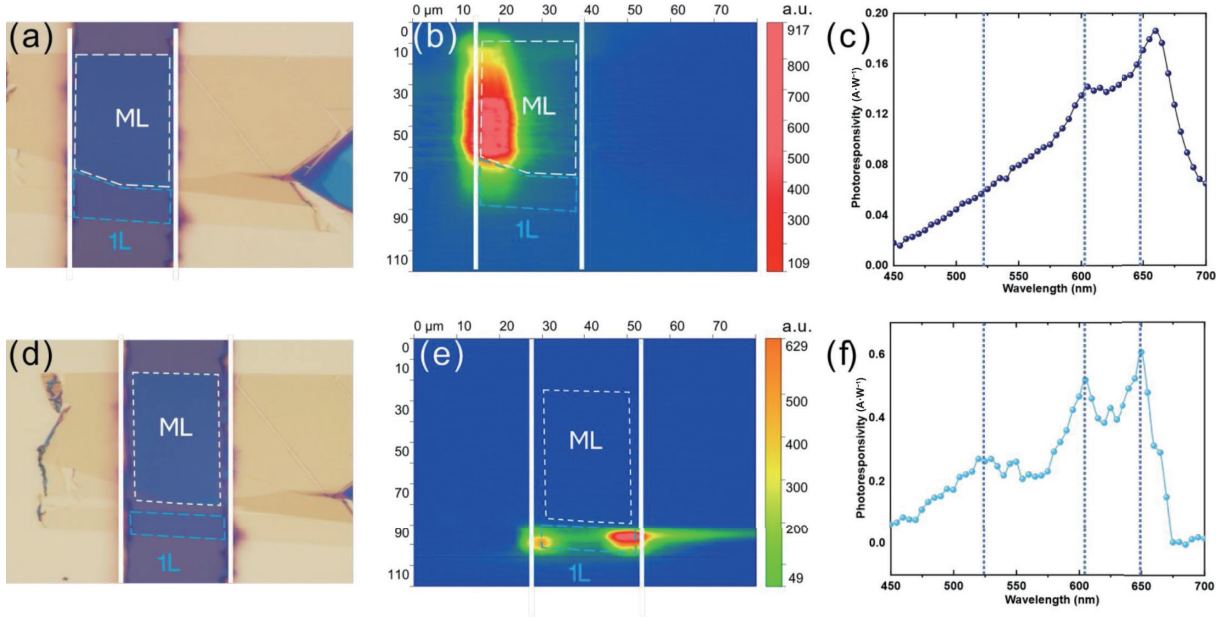

Figure 4 Optoelectronics measurements of MoS_2 device (device B) before and after laser trimming. Optical image of MoS_2 device before laser trimming (a) and after laser trimming (d). Scanning photocurrent image of MoS_2 device before laser trimming (b) and after laser trimming (e). Wavelength dependence of MoS_2 device before laser trimming (c) and after laser trimming (f).

the photocurrent is solely generated in the single-layer MoS_2 region, proving the effective isolation of the monolayer from the few layers part of the device (Fig. 4(e)). Moreover, the photocurrent spectrum now shows the A exciton peak at 650 nm, which matched the differential reflectance spectra peak of the A exciton of single-layer MoS_2 (Fig. S12 in the ESM), and a sudden drop of the photocurrent for photons with lower energy than the A exciton (as expected for a direct bandgap semiconductor as single-layer MoS_2). Interestingly, the photoresponsivity of the A exciton related peak increased from 0.2 to 0.6 $A \cdot W^{-1}$, which was attributed to the transition from the indirect band gap of bilayer to the direct band gap of monolayer MoS_2. Notice that, the increase of the photoresponsivity is also a result from the narrowed channel length from 54 μm before laser trimming to 10 μm after laser trimming (Fig. S10 in the ESM).

A WSe_2 flake was also tested with the laser trimming method using the similar process as the MoS_2 device, and we can see the effectiveness of our methodology from the contrast of the optical micrograph (Fig. S13(d) in the ESM). Therefore, we anticipate this method could be applicable to other transition metal dichalcogenides with suitable bandgap.

4 Conclusions

In conclusion, we developed a facile laser trimming method to isolate single-layers of MoS_2 from few layer regions without need of lithographic processes. It is found that laser trimming with a power of more than 6 mW can effectively separate the monolayer part of a MoS_2 from the few layer sections. We illustrate the use of this method to fabricate single-layer MoS_2 field-effect phototransistors with a completely lithography approach. We used an all dry transfer method to deposit an exfoliated single-layer MoS_2 bridging pre-patterned electrodes (deposited by shadow mask). Due to the intrinsic lack of control in mechanical exfoliation, the single-layer MoS_2 was connected to a few-layer thick region. The transfer and output curve demonstrate that the source-drain current and the photocurrent generation of the device are strongly influenced by the multilayer region. Spatially resolved photocurrent maps showed that after the laser trimming process the photocurrent is only generated at the single-layer MoS_2 region. Moreover, photocurrent spectroscopy shows a shift of the A exciton peak from 660 (expected for 2–3 layers of MoS_2) to 650 nm (in good agreement with 1L MoS_2). The results presented here will facilitate the fabrication of high performing 2D based devices for research groups without strong lithographic capabilities and provide an alternate route to reactive ion etching patterning of 2D based flakes, which could become advantageous to reduce the exposure of 2D materials to resists and solvents during fabrication.

Acknowledgements

Financial supports from the National Natural Science Foundation of China (NSFC) (Nos. 62011530438 and 61704129) are acknowledged. This work was partially supported by the Key Research and Development Program of Shaanxi (No. 2021KW-02), the fundamental Research Funds for the Central Universities (No. JB211409 and 20109215605), and the fund of the State Key Laboratory of Solidification Processing in Northwestern Polytechnical University (No. SKLSP201612).

We acknowledge funding by European Research Council (ERC) through the project 2D-TOPSENSE (GA 755655), European Union's Horizon 2020 research and innovation program (Graphene Core2-Graphene-based disruptive technologies (No. 881603) and Graphene Core3-Graphene-based disruptive technologies (No. 956813)), EU FLAG-ERA through the project To2Dox (No. JTC-2019-009), the Comunidad de Madrid through the project CAIRO-CM project (No. Y2020/NMT-6661), and the Spanish Ministry of Science and Innovation through the project (No. PID2020-118078RB-I00). O. Ç. acknowledges the European Union's Horizon 2020 research and innovation program under the grant agreement 956813 (2Exciting). S. P. acknowledges the fellowship PRE2018-084818.

Funding note: Open Access funding provided thanks to the CRUE-CSIC agreement with Springer Nature.

Electronic Supplementary Material: Supplementary material (further details of laser trimming process, optical micrograph and photocurrent, transfer and output characteristics of TMDs devices) is available in the online version of this article at https://doi.org/10.1007/s12274-022-5241-2.

References

[1] Fiori, G.; Bonaccorso, F.; Iannaccone, G.; Palacios, T.; Neumaier, D.; Seabaugh, A.; Banerjee, S. K.; Colombo, L. Electronics based on two-dimensional materials. *Nat. Nanotechnol.* **2014**, *9*, 768–779.

[2] Frisenda, R.; Navarro-Moratalla, E.; Gant, P.; De Lara, D. P.; Jarillo-Herrero, P.; Gorbachev, R. V.; Castellanos-Gomez, A. Recent progress in the assembly of nanodevices and van der Waals heterostructures by deterministic placement of 2D materials. *Chem. Soc. Rev.* **2018**, *47*, 53–68.

[3] Lemme, M. C.; Akinwande, D.; Huyghebaert, C.; Stampfer, C. 2D materials for future heterogeneous electronics. *Nat. Commun.* **2022**, *13*, 1392.

[4] Pu, J.; Takenobu, T. Monolayer transition metal dichalcogenides as light sources. *Adv. Mater.* **2018**, *30*, 1707627.

[5] Kwon, G.; Choi, Y. H.; Lee, H.; Kim, H. S.; Jeong, J.; Jeong, K.; Baik, M.; Kwon, H.; Ahn, J.; Lee, E. et al. Interaction- and defect-free van der Waals contacts between metals and two-dimensional semiconductors. *Nat. Electron.* **2022**, *5*, 241–247.

[6] Poddar, P. K.; Zhong, Y.; Mannix, A. J.; Mujid, F.; Yu, J.; Liang, C.; Kang, J. H.; Lee, M.; Xie, S. E.; Park, J. Resist-free lithography for monolayer transition metal dichalcogenides. *Nano Lett.* **2022**, *22*, 726–732.

[7] Liu, J.; Choi, G. M.; Cahill, D. G. Measurement of the anisotropic thermal conductivity of molybdenum disulfide by the time-resolved magneto-optic Kerr effect. *J. Appl. Phys.* **2014**, *116*, 233107.

[8] Jo, I.; Pettes, M. T.; Ou, E.; Wu, W.; Shi, L. Basal-plane thermal conductivity of few-layer molybdenum disulfide. *Appl. Phys. Lett.* **2014**, *104*, 201902.

[9] Kim, S. E.; Mujid, F.; Rai, A.; Eriksson, F.; Suh, J.; Poddar, P.; Ray, A.; Park, C.; Fransson, E.; Zhong, Y. et al. Extremely anisotropic van der Waals thermal conductors. *Nature* **2021**, *597*, 660–665.

[10] Zhou, Y.; Dong, Z. Y.; Hsieh, W. P.; Goncharov, A. F.; Chen, X. J. Thermal conductivity of materials under pressure. *Nat. Rev. Phys.* **2022**, *4*, 319–335.

[11] Castellanos-Gomez, A.; Barkelid, M.; Goossens, A. M.; Calado, V. E.; van der Zant, H. S. J.; Steele, G. A. Laser-thinning of MoS_2: On demand generation of a single-layer semiconductor. *Nano Lett.* **2012**, *12*, 3187–3192.

[12] Taghavi, N. S.; Gant, P.; Huang, P.; Niehues, I.; Schmidt, R.; de Vasconcellos, S. M.; Bratschitsch, R.; García-Hernández, M.; Frisenda, R.; Castellanos-Gomez, A. Thickness determination of MoS_2, $MoSe_2$, WS_2 and WSe_2 on transparent stamps used for deterministic transfer of 2D materials. *Nano Res.* **2019**, *12*, 1691–1695.

[13] Castellanos-Gomez, A.; Buscema, M.; Molenaar, R.; Singh, V.; Janssen, L.; van der Zant, H. S. J.; Steele, G. A. Deterministic transfer of two-dimensional materials by all-dry viscoelastic stamping. *2D Mater.* **2014**, *1*, 011002.

[14] Liu, Y.; Guo, J.; Zhu, E. B.; Liao, L.; Lee, S. J.; Ding, M. N.; Shakir, I.; Gambin, V.; Huang, Y.; Duan, X. F. Approaching the Schottky-Mott limit in van der Waals metal-semiconductor junctions. *Nature* **2018**, *557*, 696–700.

[15] Reuter, C.; Frisenda, R.; Lin, D. Y.; Ko, T. S.; de Lara, D. P.; Castellanos-Gomez, A. A versatile scanning photocurrent mapping system to characterize optoelectronic devices based on 2D materials. *Small Methods* **2017**, *1*, 1700119.

[16] Riccardo, R.; Yue, N.; Gant, P.; Molina-Mendoza, A. J.; Schmidt, R.; Bratschitsch, R.; Liu, J. X.; Fu, L.; Dumcenco, D.; Kis, A. et al. Micro-reflectance and transmittance spectroscopy: A versatile and powerful tool to characterize 2D materials. *J. Phys. D: Appl. Phys.* **2017**, *50*, 074002.

[17] Yang, R.; Zheng, X. Q.; Wang, Z. H.; Miller, C. J.; Feng, P. X. L. Multilayer MoS_2 transistors enabled by a facile dry-transfer technique and thermal annealing. *J. Vac. Sci. Technol. B* **2014**, *32*, 061203.

[18] Radisavljevic, B.; Kis, A. Mobility engineering and a metal-insulator transition in monolayer MoS_2. *Nat. Mater.* **2013**, *12*, 815–820.